

Pion double-charge exchange on ^{16}O and ^{18}O

R. L. Burman, M. P. Baker, M. D. Cooper, R. H. Heffner, D. M. Lee, R. P. Redwine, and J. E. Spencer
Los Alamos Scientific Laboratory, Los Alamos, New Mexico 87545

T. Marks, D. J. Malbrough, and B. M. Freedom
University of South Carolina, Columbia, South Carolina 29208

R. J. Holt and B. Zeidman
Argonne National Laboratory, Argonne, Illinois 60439
 (Received 31 October 1977)

The zero-degree differential cross section for pion double-charge exchange on $^{18}\text{O}(\pi^+, \pi^{+-})^{18}\text{Ne}$ was measured at three incident pion energies and found to be 2.00 ± 0.34 , 2.19 ± 0.44 , and 1.67 ± 0.38 $\mu\text{b}/\text{sr}$ at 139, 126, and 95 MeV, respectively. A similar measurement for ^{16}O at an energy of 145 MeV resulted in a value of 0.87 ± 0.21 $\mu\text{b}/\text{sr}$. The ratio of the ground-state transitions near 140 MeV is $\sigma(^{18}\text{O})/\sigma(^{16}\text{O}) = 2.3 \pm 0.7$. The mass excess determined for ^{16}Ne is 24.4 ± 0.5 MeV. The experimental setup and data analysis are discussed in detail. Results are compared with various calculations and discussed from the standpoint of their implications for learning about reaction dynamics and nuclear structure. The reaction appears to be quite sensitive to ground-state correlations of the target.

$$\left[\begin{array}{l} \text{NUCLEAR REACTIONS } ^{18}\text{O}(\pi^+, \pi^-), E=95\text{--}139 \text{ MeV; measured } \sigma(E, \theta=0^\circ). \\ ^{16}\text{O}(\pi^+, \pi^-), E=145 \text{ MeV; measured } \sigma(\theta=0^\circ), \text{ deduced } \Delta M(^{16}\text{Ne}). \end{array} \right]$$

I. INTRODUCTION

Discussions¹ of pion double-charge exchange date back to the early 1960's, and calculations² began to appear in the mid 1960's. Much of that work was prompted by the discovery of isobaric analog states with the (p, n) reaction³ and the possibility of exciting the hypothetical double isobaric analog with pions in much the same manner. In the period between 1964 and 1968, three experimental searches for pion double-charge exchange (DCE) to two-body final states were performed.⁴ In all of these experiments, the incident beam resolution was ≈ 4 MeV full width at half maximum (FWHM) and the intensity was $\leq 5 \times 10^5/\text{s}$. Although generally unsuccessful, they were able to successively decrease the upper limits on the cross sections to levels of about 1 $\mu\text{b}/\text{sr}$ —a result considerably lower than predicted by the early calculations. During this same period, states with $T = T_z + 2$ were observed and shown to be narrow,⁵ but there were no further attempts at DCE because of the extreme difficulty of the experiments. Thus, although pion DCE had been studied both experimentally and theoretically since the early 1960's, neither analog ($\Delta T = 0$) nor ground-state transitions ($\Delta T \geq 0$) had been observed before 1976.

With the significantly higher intensities becoming available at meson factories, successful experiments investigating pion single- (Ref. 6) and double- (Refs. 7–9) charge-exchange transitions to

discrete final states have now been performed. In this paper, we present the complete results of the first pion DCE experiment in which both analog⁷ and nonanalog⁸ transitions were observed. In order to maximize the probability of a successful result, the experiment was performed at zero degrees. The experiment and data analysis are first discussed in detail followed by a comparison of the results to the most recent predictions.^{10–12} Finally, the conclusions and implications for future experiments are discussed.

II. EXPERIMENT

The experiment was carried out on the low-energy pion (LEP) channel at the Los Alamos Meson Physics Facility. The LEP channel is an isochronous, four-bend vertical system¹³ shown in the upper half of Fig. 1. The charge-exchange targets were placed at the channel midpoint, and the two halves of the channel were tuned for opposite polarities. In this configuration the channel served as both pion channel (π^+) and zero-degree spectrometer (π^-). A detection system at the downstream end of the spectrometer, shown schematically in the lower half of Fig. 1, was used to identify the transmitted particles and to determine their momentum by measuring their location along the focal plane. For this experimental setup, the real data rate for the (π^+, π^-) reaction was typically $\approx 3/h/(\mu\text{b}/\text{sr})/(\text{g}/\text{cm}^2)$ for an average proton current of 100 μA .

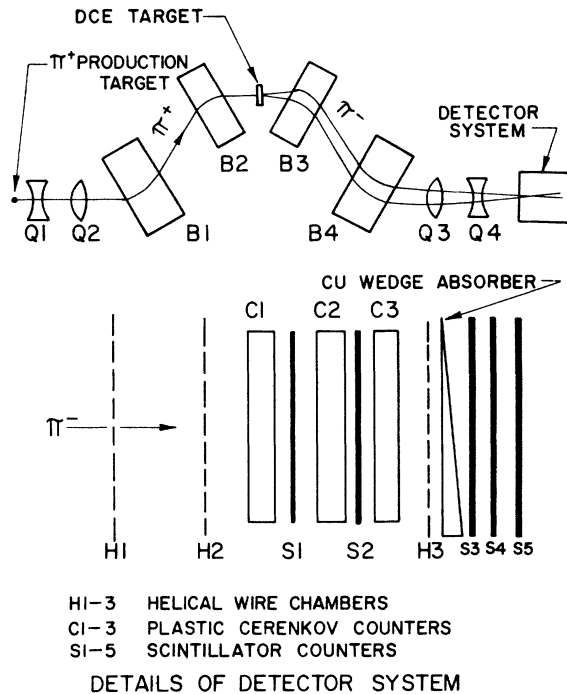


FIG. 1. Schematic layout of the LAMPF low-energy pion channel and DCE spectrometer.

There are a number of practical advantages in running the experiment at an angle of 0° . For example, the primary π^+ (or π^-) beam can be sent directly through the spectrometer to measure the resolution, efficiency, and incident pion flux with exactly the same configuration as used during the experiment. The target thickness can be increased (with poorer resolution) without necessarily lowering the quality of the resulting data. Although increasing the target thickness may not improve the signal-to-noise ratio, it does increase the real event rate which we expected to be a maximum at 0° for the cross sections of interest.

A. LEP channel

Pions were produced from a 3-cm-thick carbon target with a beam of 800-MeV protons. During this experiment, the proton beam averaged $100\ \mu\text{A}$ with a 6% duty factor.

The arrangement of the bending magnets $B1$ and $B2$ and quadrupoles $Q1$ and $Q2$ is such that they present a horizontally and vertically focused beam which is vertically dispersed in momentum along the plane of symmetry (midplane of channel and location of DCE target as shown in Fig. 1). The momentum bite ($\delta p/p$) is selected by means of a set of collimators allowing an adjustable vertical gap at the midplane. A 3-cm opening of the slits, corresponding to a momentum bite of 1.0%, was

used for all of the present experiments. With this setting and the proton flux available, the pion flux at the target was typically $\approx 2 \times 10^7/\text{s}$ depending on the incident pion energy.

The ^{18}O target was a 7-cm-diam by $3.44\text{-g}/\text{cm}^2$ gelatin target mounted in a Lucite frame. The gelatin, with a 1.5% by weight admixture of agar-agar, was made from water enriched to 91% ^{18}O . The ^{16}O target was similar but slightly thinner, $3.28\text{ g}/\text{cm}^2$, and made of natural water (99.76% ^{16}O). These targets were placed in the proton absorber wheel located immediately downstream of the momentum slit and could be changed remotely.

The downstream half of the channel, which approximately acted as an energy-loss spectrometer, was tuned for negative pions. The acceptance solid angle for the spectrometer was about 7.2 msr and was determined by Monte Carlo simulation. The dynamic range of the spectrometer was determined by the same technique; e.g., particles of momenta different from the spectrometer's central momentum were traced through the second half of the channel to establish the solid-angle dependence on particle momentum. The results presented in Table I indicate that the system does not vary significantly over the central 8 MeV of energy acceptance.

B. Background

With the channel tuned to the (+, -) mode, there are two major sources of background expected: electrons, and negative pions produced from (n, π^-) reactions along the channel and in the target. These pions have a wide range of energies and trajectories and are thus nearly uniformly distributed in energy. Because of the absence of any sharp energy structure to this background, a peak from the DCE reaction should stand out. Also, since the neutrons have different energies and travel different paths, the time-of-flight (TOF) of the resulting pions should be uniformly distributed within the 5-ns period of the accelerator rf structure in contrast to a peak in the time spectrum of

TABLE I. Spectrometer acceptance solid angle as a function of pion momentum.

$(P-P_0)/P_0$ (%)	Solid angle (msr)
0	7.2
1	7.3
2	7.3
3	7.2
4	7.0
5	6.6
6	5.9

the DCE pions.

Electrons are the dominant source of background. They arise primarily from $e^+ \rightarrow \gamma \rightarrow e^-$ conversions in the target; with the 3.44-g/cm² ¹⁸O target, a π^+ energy of 143 MeV, and the spectrometer set for 130-MeV negative pions, the calculated electron rate was about 10⁴/h. Our measurements yielded a value of several times 10⁴/h, in reasonable agreement with the calculations. Electrons are also produced as a result of pion single-charge exchange and the resulting π^0 decay; the electron background from this source was calculated to be lower by about a factor of 5 than the $e^+ \rightarrow \gamma \rightarrow e^-$ conversion.

C. Detector system

The detector system shown in the lower half of Fig. 1 was designed to be efficient for detecting pions and extremely efficient for vetoing electrons because of the large ratio of $e:\pi \approx 10^3:1$. Two helical wire chambers, placed at the front of the detector stack, were used to determine the intersection of a particle's trajectory with the focal plane and were capable of providing an energy resolution of 0.5 MeV (FWHM) at 140 MeV. Three independent 3.8-cm-thick Lucite Čerenkov counters with photomultiplier tubes on each end were used to reduce the possibility of false triggers from processes such as $e \rightarrow \gamma \rightarrow e$ showers. The two 1.3-cm-thick plastic scintillation counters, S1 and S2, interspersed with C1-C3, were smaller than the Čerenkov counters (10 cm by 40 cm, and 12.5 cm by 42.5 cm, respectively) to avoid geometrical problems from slight misalignment.

The gains and thresholds on the Čerenkov counters were set such that each end was about 99% efficient for detecting normally incident electrons. This procedure resulted in about 98% electron efficiency when signals from both ends of any Čerenkov counter were required to be in coincidence. Most of the good pion events did not fire both ends of any of the Čerenkov counters. Thus valid pion events were recorded by an event trigger defined by $S1 \cdot S2 \cdot S3$ with no Čerenkov counter firing on both ends. The resulting rejection of good pions (less than 25%) was measured using a π^+ beam with the channel in the (-, -) mode so that efficiency corrections could be made following analysis. Analog information corresponding to the light output from each end of the three Čerenkov counters was also recorded for each event. Random and background events were monitored with other combinations of Čerenkov and scintillator coincidences.

Scintillation counter S1 was also part of a TOF system to measure particle arrival time relative

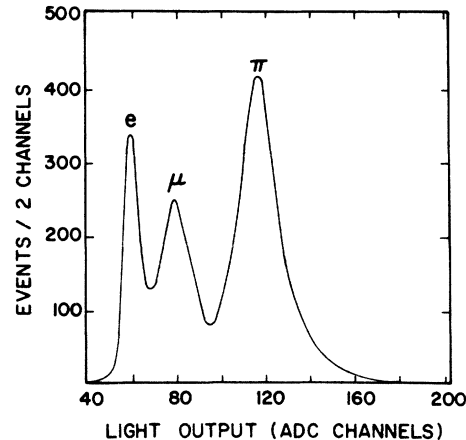


FIG. 2. Particle spectrum in the S3 scintillator detector. A clear separation is observed between pions and electrons.

to the accelerator rf microstructure. Counters S3-S5 provided some discrimination between electrons and pions on the basis of differential energy loss. To achieve good separation between pions and electrons in the back scintillators, the pions entering S3 were degraded to about 40 MeV with a copper absorber. Because pions coming from the spectrometer are vertically dispersed, the absorber was in the shape of a wedge to roughly equalize the energy of the pions incident on S3. Operated in this way, the detector stack efficiency was uniform to $\pm 5\%$ over the central ± 5 MeV acceptance of the spectrometer. Figure 2 shows a typical spectrum for S3.

D. Beam monitoring

The number of pions incident on the DCE targets was calibrated to the flux of protons incident on the pion production target. The proton current was measured with a toroid upstream of the production target. To relate the number of pions incident on the DCE target to the proton measurements, the activation technique described below was used.

Because the DCE target region was inaccessible during the runs, the pion flux was measured at the end of the channel and corrected to the midpoint using the channel acceptance and pion decay factor. The channel was tuned to the (+, +) mode and set for a pion energy equal to that used during the experiment. The ratio of the proton toroid count to the pion flux had been investigated in several experiments and found to be constant to better than 3% over periods of 12 hours.

A plastic scintillator disk, placed at the end of the channel, was activated for a fixed time using the $^{12}\text{C}(\pi^+, \pi^+n)^{11}\text{C}$ reaction. The induced activity (half-

life 20.8 min) from the β decay of ^{11}C was then measured. With the known cross section for this reaction,¹⁴ the pion flux per proton toriod count could then be determined and used to normalize the DCE measurement. Activation measurements were done for each incident π^+ energy and the results agreed well with expected rates.

III. DATA ANALYSIS AND RESULTS

The data were read and recorded on magnetic tape using a DEC PDP-11/45 computer. For each event, the following signals were recorded: light output from each scintillator, light output from each end of the three Čerenkov counters, timing information from each end of the anode and cathode of the three helical wire chambers, the time between the S1 signal and the accelerator rf pulse, and a bit pattern showing which Čerenkov signals exceeded a preset threshold. Each event carried with it a data word identifying which hardware trigger initiated the recording of the event.

A. Spectrometer energy calibration

The first two helical wire chambers at the exit of the spectrometer were used to determine the particle's trajectory and hence its momentum. The chambers were calibrated using a collimated ^{55}Fe source and a jig to position the source accurately on each chamber. The origin of the coordinate system for each chamber was determined by putting a 130-MeV pion beam completely through the channel and spectrometer.

The orientation and location of the focal plane were checked experimentally as follows. With the ^{18}O target in place, calibration data were taken in the $(-, -)$ mode for a fixed spectrometer setting and five different incident pion momenta in the range $p = p_0 \pm 3\%$. Trajectories for approximately 100 particles were plotted for each momentum. Neither a rotation nor a translation of the focal plane away from the expected values significantly improved the resolution. The momentum dispersion predicted by a TRANSPORT¹⁵ calculation was verified in this way.

The intrinsic resolution of the spectrometer (0.4 MeV FWHM) was limited mostly by multiple scattering in the channel windows and wire chambers. After the ^{18}O target was inserted and the upstream half of the channel tuned to a higher energy to compensate for the energy loss in the target (~ 8 MeV), the resolution was measured to be ~ 4 MeV FWHM. This degradation of the resolution was due to multiple scattering and energy straggling in the thick target.

B. Time of flight

The TOF was used to discriminate against background by aiding in the identification of electrons and asynchronous pions. It was measured by the time difference between S1 · S2 · S3 (leading edge timing given by S1) and the accelerator rf pulse. Since the proton beam microstructure consisted of 0.25-ns pulses separated by 5.0 ns, the time difference could only be measured modulo 5 ns, thus producing a TOF spectrum folded into a single 5-ns range. Corrections were then applied for variations in S1 timing due to different pulse heights and for the propagation time through S1 due to different particle locations along S1. Since the wire chambers at the exit of the spectrometer determined particle position and angle, it was also possible to correct for the calculated path length through the spectrometer. When all of these corrections were made, the TOF resolution was about 700 ps FWHM.

C. Counter stack efficiency

A sizable fraction of pions was lost due to reactions before counter S3. These reaction losses were calculated using total pion-nuclear cross sections and were found to be as large as 50%. Pion losses due to multiple scattering out of the stack and decay in flight were also calculated and found to be on the order of 5–10%. The corrections to the DCE cross sections resulting from the loss of pions, including the fraction due to Čerenkov rejection, were, however, measured directly with the beam.

In order to make this efficiency test under conditions very similar to the data runs, the channel was set in a $(-, -)$ mode with the ^{18}O target in place so that the emerging beam had an energy and geometry similar to the pions in the DCE experiment. A large number of events were then recorded based only on an S1 trigger requirement. Pions were selected by applying cuts on TOF and pion energy in the S1 counter. Muons in the beam were identified in the pulse-height spectrum in S5. It was then only necessary to determine the loss of pions between S1 and S3. Pions which decayed or were lost through reactions were automatically accounted for by the S3 cut. In order to determine the pion loss due to Čerenkov rejection, it was necessary to look at the bit pattern of Čerenkov counters for those pions which survived the S3 cut. Depending on the energy, typically >77–93% of the pions did not trigger any Čerenkov counter and 96–100% did not trigger any two of the three. The pion loss before S1, i.e., in C1, could be estimated from the measured loss in C2.

TABLE II. Pion loss due to reactions, multiple scattering, and Čerenkov rejection.

Incident pion energy (MeV)	Percentage of pions lost due to reactions and multiple scattering		Measured pion losses including Čerenkov rejection (%)
	Calculated	Measured	
130	61	55	64
116	55	51	58
86	40	39	43

The results of these calculations and measurements are shown in Table II.

D. Cross-section extraction

As mentioned before, all of the events used to extract cross sections were triggered by a triple coincidence, $S1 \cdot S2 \cdot S3$, with no veto by any one of three Čerenkov counters. The requirement of signals in both front helical wire chambers, and a loose cut on the pulse height of scintillator S3 to eliminate some electrons, gives a two-dimensional energy-vs-TOF spectrum such as shown in Fig. 3(a). The only other cut required was one on TOF. The limits for this cut were known *a priori* from the efficiency test; as shown in Fig. 3(b), a TOF cut of 1.0 ns clearly separates pions and electrons and reduces by four-fifths the asynchronous background. The pion energy spectrum shown in Fig. 3(c) was obtained from the spectrum of Fig. 3(a) after making the TOF cut.

In order to investigate DCE to the continuum, the spectrometer setting was changed while leaving the pion channel setting fixed at 139 MeV. Two spectrometer settings, 124 and 116 MeV, were taken in addition to the original 130-MeV setting. After making cuts similar to those applied to the 130-MeV data and correcting for monitor counts, stack efficiency, and the spectrometer transmission efficiency, the spectrum in Fig. 4 was obtained.

The background from all sources other than target-associated DCE was measured by replacing the ^{18}O target by a similar ^{16}O target. Since the Q value for DCE on ^{16}O is at least 20 MeV more negative than that for ^{18}O , all sources of events from everything but ^{18}O are present. After making the rather small subtraction indicated by the dotted line in Fig. 4, there was a net number of 242 events in the DCE peak which gave a cross section of $2.0 \pm 0.34 \mu\text{b}/\text{sr}$. The effect of the various corrections described above on the cross section are listed in Table III. The value of the cross section quoted here differs from that of Ref. 7 in order to account for pion absorption in the DCE

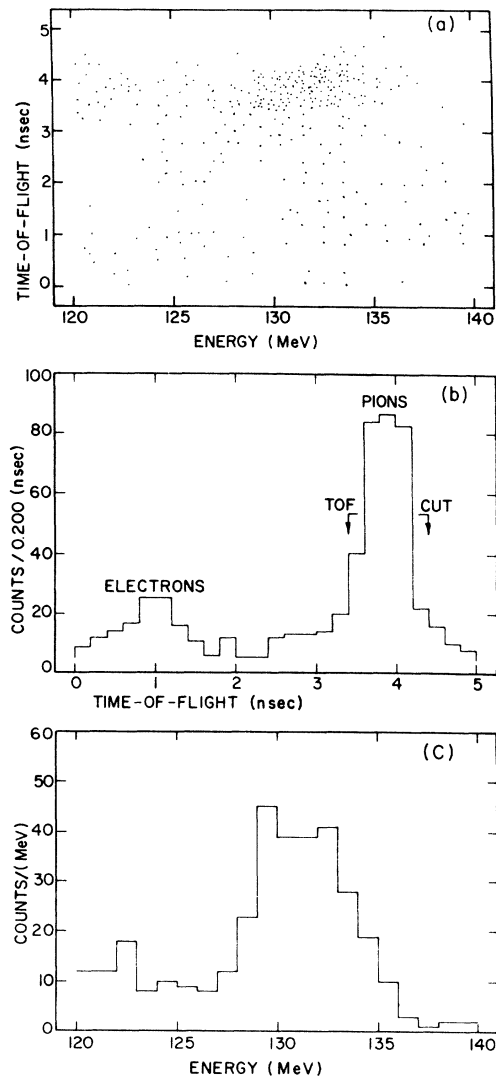


FIG. 3. Data at an incident mean pion energy of 139 MeV and a spectrometer setting of 130 MeV for events surviving the Čerenkov and scintillator electron rejection: (a) scatter plot of energy vs TOF; (b) projection on the TOF coordinate, showing a small residual electron band and very little (less than 5%) asynchronous background; (c) projection [after making TOF cut shown in (b)] on the energy coordinate, showing a peak at 130.7 MeV at the expected location of the ^{18}Ne ground state.

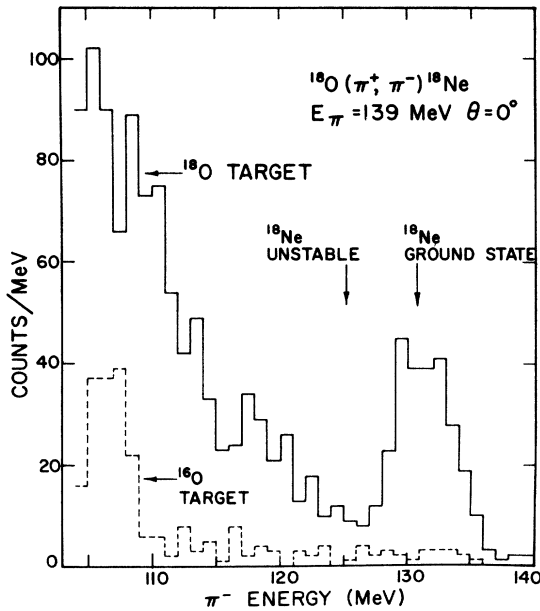


FIG. 4. Combined π^- spectra for three spectrometer settings. The DCE isobaric analog transition to the ^{18}Ne ground state is clearly separated from the continuum. The dashed line shows a small background, as measured with an ^{16}O target.

target.

The Q value for the $^{16}\text{O}(\pi^+, \pi^-)$ reaction was estimated from mass systematics to be about -28 MeV. Just above the low-energy cutoff of the spectrometer at the lowest energy shown in Fig. 4, a sudden rise in the cross section for the ^{16}O target can be seen. With the spectrometer set at 112 MeV and the channel reset to 149 MeV, the spectrum of Fig. 5 was obtained for the reaction $^{16}\text{O}(\pi^+, \pi^-)^{16}\text{Ne}$. The peak in the spectrum is superimposed upon a low, presumably constant background, similar to that in Fig. 5, and another energy-dependent background that is assumed to

come from breakup reactions yielding multiparticle final states. After subtracting the background indicated on the figure, 134 events remained, giving a cross section of $0.87 \pm 0.21 \mu\text{b}/\text{sr}$.

Additionally, cross sections were determined for the reaction $^{18}\text{O}(\pi^+, \pi^-)^{18}\text{Ne}$ at mean incident energies of 95 and 126 MeV. The spectrum taken at 95 MeV is shown in Fig. 6 and the complete results for both ^{16}O and ^{18}O are summarized in Table IV. For the lower-energy measurements, the location of the low-energy cutoff of the peak is not as obvious because of poorer statistics and larger backgrounds. Using the expected location of the centroid and the shape of the high-energy side of the peak, the low-energy cutoff was determined in a consistent way for all energies. In addition, a systematic uncertainty in the number of events was assigned due to the uncertainty in the location of the low-energy cutoff. These uncertainties were ± 10 and ± 20 events for the 126- and 95-MeV runs, respectively. For the cross section on ^{16}O , the assumed background shape was varied to establish a similar systematic uncertainty in the net number of events.

E. ^{16}Ne mass excess

In the spectrum of Fig. 6 for the $^{16}\text{O}(\pi^+, \pi^-)^{16}\text{Ne}$ reaction, a distinct peak is observed near the energy predicted on the basis of mass systematics.¹⁶ After subtraction of background as shown, the centroid of the observed peak yields a mass excess for ^{16}Ne of 24.4 ± 0.5 MeV. The width of the peak (FWHM) is 5 MeV, mostly due to multiple scattering and energy straggling in the thick H_2O target and the intrinsic width of the unbound ground state of ^{16}Ne . The energy calibration was obtained by sending π^- beams, of several energies that spanned the acceptance range, through the spectrometer when it was tuned for a central value of

TABLE III. Cross section corrections and errors (for ^{18}O target at a mean incident π^+ energy of 139 MeV).

Counter stack efficiency	0.36 ± 0.03	8%
Statistical error in pion sample (4%)		
Loss in Čerenkov counter 1 (2%)		
Muon contamination (3%)		
Uncertainty in S3 cut (2%)		
Spectrometer solid angle	$7.2 \pm 0.4 \text{ msr}$	6%
Relative spectrometer transmission	0.95 ± 0.02	2%
Activation run vs data run		
Uncertainty in pion monitor		10%
Uncertainty in number of target nuclei		3%
Statistical error in N_{π^-} in DCE peak		8%
Pion flux loss in target	0.11	2%
Total error		16%

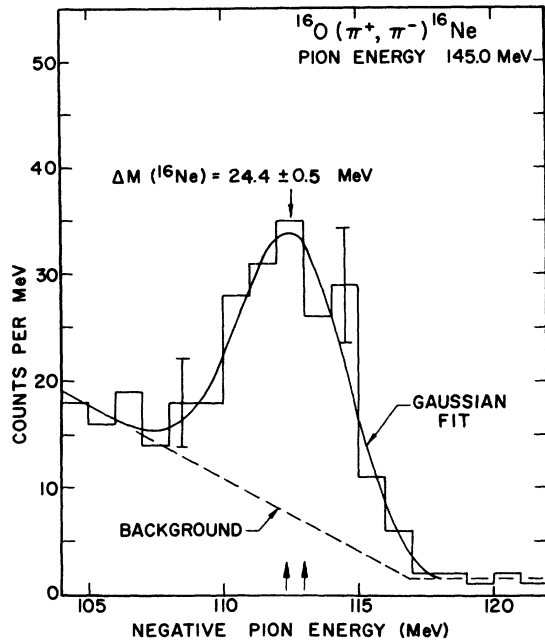


FIG. 5. Spectrum of the $^{16}\text{O}(\pi^+, \pi^-)^{16}\text{Ne}$ reaction at 0° for a mean energy of 145 MeV. The arrow at the peak indicates the centroid after background subtraction. The arrows on the abscissa are theoretical predictions.

112 MeV. The error in the mass excess is primarily due to uncertainties from the energy calibration and from the assumed shape of the energy-dependent background.

The calculations based upon mass systematics predict¹⁶ mass excesses of 24.11 and 24.67 MeV. Preliminary (^4He , ^8He) reaction data favor the lower of these values.¹⁷ Within errors, the value measured here, $\Delta M = 24.4 \pm 0.5$ MeV, is in agreement with either predicted mass excess for the ground state of ^{16}Ne . It is interesting that Ericson suggested this experiment as an example of the utility of pion DCE reactions in one of the early written discussions on the subject.¹

IV. THEORETICAL BACKGROUND

Only quite recently have precision measurements of pion-induced reactions on complex nu-

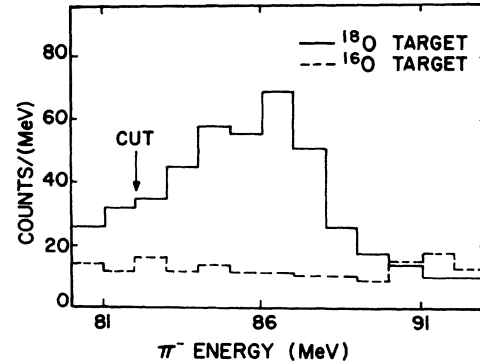


FIG. 6. Spectrum of the $^{18}\text{O}(\pi^+, \pi^-)^{18}\text{Ne}$ reaction at 0° for a mean energy of 95 MeV. The background, as measured with an ^{16}O target, is shown as a dashed curve. The definition of the low-energy side of the peak is shown by the arrow.

clei been performed. Given this dearth of experimental results, the various theoretical approaches have had little data available with which to check their predictions. Consequently, these calculations, particularly for DCE, should be interpreted as more qualitative than quantitative. In the following sections, the theoretical background for the DCE experiment is reviewed, and the latest versions of some calculations are presented.

A. Zero-degree considerations

The *a priori* expectation that measurement at zero degrees is optimal was based upon several theoretical considerations. These arguments strongly imply that (1) the ($0^+ \rightarrow 0^+$) ground-state channel dominates the transitions to low-lying levels in both the ^{18}O and ^{16}O reactions, and (2) the zero-degree differential cross section is representative of the double-analog-state-reaction cross section for ^{18}O .

Figure 7 shows some results of a realistic calculation for ^7Li single-charge exchange (SCE)¹⁸ which are in reasonable agreement with the available data. The initial state has $\frac{3}{2}^-$, and the cross section sums the first two states in ^7Be , the analog ($\frac{3}{2}^-$), and first excited state ($\frac{1}{2}^-$), corre-

TABLE IV. Summary of cross sections.

Target	Mean incident π plus energy (MeV)	Number of events in DCE peak	Number of background events	Cross section ($\mu\text{b}/\text{sr}$)
^{18}O	139	264 ± 16	22 ± 5	2.00 ± 0.34
^{18}O	126	143 ± 16	14 ± 4	2.19 ± 0.44
^{18}O	95	372 ± 28	130 ± 17	1.67 ± 0.38
^{16}O	145	134 ± 25	...	0.87 ± 0.21

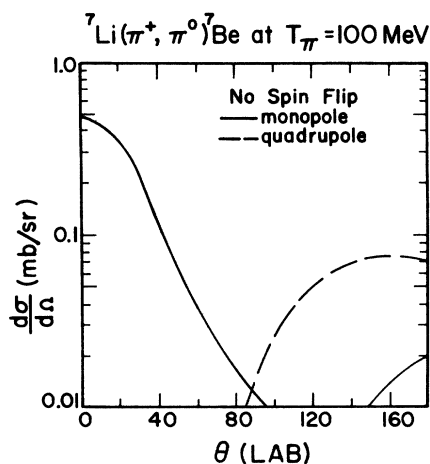


FIG. 7. Fixed-scatterer calculation of Ref. 18 for SCE on a nonzero-spin target in the no spin-flip approximation. The dominance of the monopole transition at 0° is evident.

sponding to the experimental data.⁶ When spin-flip is ignored, the $\frac{3}{2}^- \rightarrow \frac{1}{2}^-$ cannot occur via a monopole transition whereas the $\frac{3}{2}^- \rightarrow \frac{3}{2}^-$ ground-state transition can go by both monopole and quadrupole transitions. The integrated cross sections are 0.61 mb for the monopole and 0.32 mb for the quadrupole. While these are comparable, the 0° cross sections are totally different with the monopole completely dominating. Similarly, for zero-spin targets, the transition multipolarity is determined by the spin of the final level (J_f). As a result, the $^{18}\text{O}(\pi^+, \pi^0)^{18}\text{F}(0^+)$ SCE reaction to the analog should be forward peaked while transition strength with $J_f \neq 0$ should be negligible at 0° until level densities increase sufficiently. Since the $^{18}\text{F}(0^+)(\pi^0, \pi^-)^{18}\text{Ne}(0^+)$ reaction should proceed with the same amplitude, the ^{18}O DCE reaction at 0° would dominantly excite only the ground-state double analog in the coherent scattering approximation^{11,12} in which the nucleus always remains within the ground-state isospin multiplet. Specifically, the 2_1^+ level at 2.0 MeV, which is not completely resolvable in our experiment, should contribute very little at zero degrees since it must go by a quadrupole transition.

These arguments are based on a complete multiple-scattering calculation of pion SCE¹⁸ which included inelastic excitations of the core in both initial and final channels to all orders. A simpler and more physical argument, which leads to the same conclusions, may be obtained from realistic calculations of pion elastic and inelastic scattering,¹⁹ which predict the selective excitation of higher spin states with increasing momentum transfer. This has been verified experimentally with other probes such as electrons and protons

and is based on the fact that larger angular-momentum transfers (L) result from larger linear-momentum transfers for surface-peaked reactions ($L \sim qR_N$, where q is the linear momentum transfer and R_N the nuclear radius). In plane-wave approximation, transitions of multipolarity L will peak according to the spherical Bessel function of order $L (= J_f)$. Similarly, at $\theta = 0^\circ$, the monopole peaks and is the only multipole which is nonzero at $q = 0$. For the 0° reaction $^{18}\text{O}(\pi^+, \pi^-)^{18}\text{Ne}(g.s.)$ with an incident kinetic energy greater than 80 MeV, the momentum transfer $q \sim 8$ MeV/c so that $qR_N \sim 0.1$. For ^{16}O , the corresponding numbers are $q \sim 40$ MeV/c and $qR_N \sim 0.6$. Thus, 0° is in the semiclassically forbidden region of L transfers for all $L > 0$ for both ^{16}O and ^{18}O . Such suppositions must ultimately be confirmed experimentally, and a recent spectrum obtained at SIN⁹ for ^{18}O at $\theta = 18^\circ$ and $T = 148$ MeV appears to show little excitation of the 2^+ state.

When there are several partial waves contributing, the angular distribution will usually be a maximum at 0° . Similarly, one also expects that the cross section at this angle would be the one

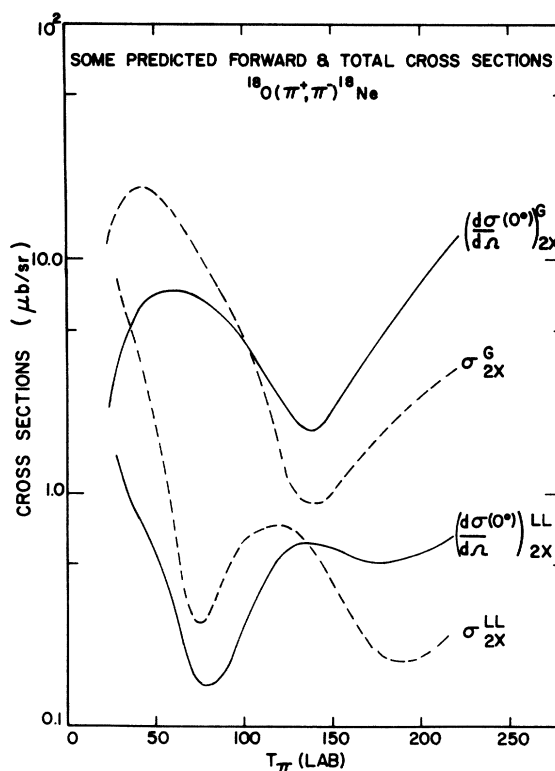


FIG. 8. Comparison of Glauber model (Ref. 11, labeled G) and optical-model (Ref. 12, labeled LL) predictions of DCE cross sections as a function of energy. Zero-degree differential cross sections are denoted by solid lines, total cross sections by dashed lines.

to most nearly parallel the integrated reaction cross section to the ground-state analog, even though there is no necessary relationship between the two. Figure 8 shows the correspondence between these two cross sections predicted by Glauber¹¹ and optical-model calculations¹² for elastic DCE. Although the two types of calculations give results that differ widely in both magnitude and structure, the overall trend between the two cross sections in each model is similar, with $d\sigma(0^\circ)/d\Omega$ mirroring the integrated cross section. Thus, it may be reasonable to infer the trend of the reaction cross section from the 0° cross section, especially since it is more easily measured and less subject to error.

B. Predictions

Before this experiment, only upper limits were established⁴ for the elastic DCE reaction on a few nuclei such as ^7Li , ^{51}V , and ^{90}Zr . Furthermore, there was also a total absence of any elastic, SCE, or DCE data on either ^{16}O or ^{18}O over the range of interest. Thus, because the experimental input for calculations was minimal, theoretical studies of DCE were concerned not with fine details but more with determining the sensitivity of the re-

action to various parameters. Figure 9 illustrates the situation prior to the experiment by showing the various predictions which were available for $d\sigma(0^\circ)/d\Omega$ vs pion energy.

The calculations are bounded on the lower side by the coupled channel optical-model calculations of Miller and Spencer¹² and on the upper side by the plane-wave Born calculations of Parsons, Trefil, and Drell.² These differ by as much as two orders of magnitude, and the source of the discrepancy was argued¹² to result from the plane-wave calculation not properly taking into account the absorption from the nuclear many-body system. Thus, the elastic DCE cross section to the double analog would essentially follow the basic $p(\pi^-, \pi^0)n$ cross section, which is a broad bump over the (3, 3) resonance were it not for nuclear absorptive effects. The optical-model calculations indeed show a broad dip due to increasing competition from such processes with increasing energy. Furthermore, within the optical-model work, it was shown¹² that although the DCE calculations were quite sensitive to the off-shell extrapolation assumed for the optical potential (Kisslinger or local Laplacian), there was essentially no modification to the first-order potential that could change this overall trend with energy.

However, the most remarkable aspect of Fig. 9 is perhaps the factor of 30 difference between the calculations of Refs. 10–12 which were the most detailed calculations carried out. All of them were based on some form of multiple-scattering theory which was calculated to all orders. Each assumed ^{18}O to be an ^{16}O core plus two neutrons in the $1d_{5/2}$ orbital and that the ^{18}Ne final state was identical except for the change of neutrons to protons outside the core. Each used harmonic oscillator densities based on electron-scattering measurements corrected for the finite size of the proton as well as pion-nucleon (πN) phase shifts. While one could argue that the reaction is sensitive to higher-order processes, such as ground-state correlations, the large variations between the different results indicate considerable sensitivity to the basic approximation made in the individual models so that caution is required before drawing definite conclusions.

The Glauber calculations of Liu and Franco¹¹ should most nearly correspond to the first-order coupled optical equations computed with the local Laplacian potential. However, as shown in Fig. 8, there seems to be little similarity between the two, either in structure or magnitude. The major source of the difference results from the πN s - p wave cancellation in the isospin-dependent part of the potential. It is necessary to first reconcile such model differences before conclusions are

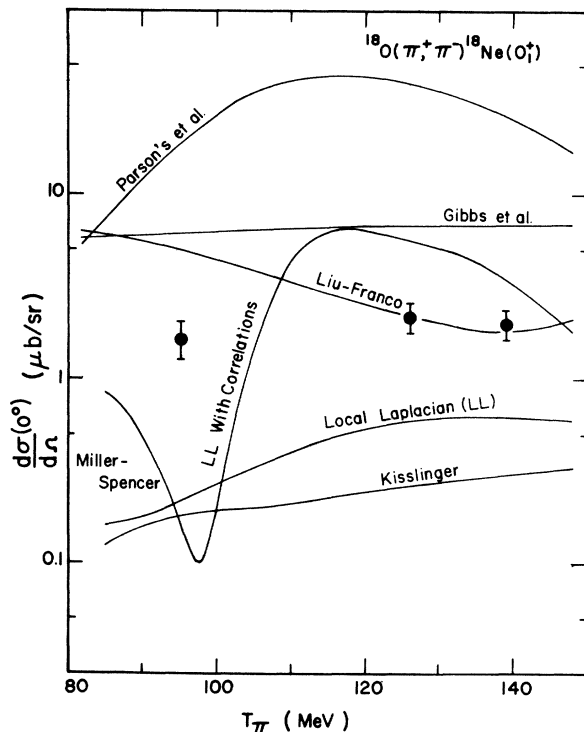


FIG. 9. Estimates of the zero-degree differential cross section for pion charge exchange to the double analog which were available prior to the experiment. The data shown are from this experiment.

made about the form of the first-order optical potential appropriate to elastic, inelastic, or charge-exchange processes. However, since these models describe elastic scattering in the πN resonance region comparably well, it is possible that charge-exchange reactions may provide the clearest tests of the various model assumptions.

The fixed-scatter calculation of Gibbs, Gibson, Hess, and Stephenson¹⁰ is an adaptation of Watson's multiple-scattering theory in which the pion amplitude is obtained exactly and then averaged over the specific nuclear density by means of a Monte Carlo technique. Consequently, it is limited in practice to nuclei with $A < 20$.

We have included the results of the experiment in Fig. 9 to illustrate that although the predictions bracket the data, all of them fail to reproduce the results.

C. Recent theoretical calculations

The publication of the initial results of the present experiment⁷ has stimulated a reexamination of the calculations. Other pion reaction data in this

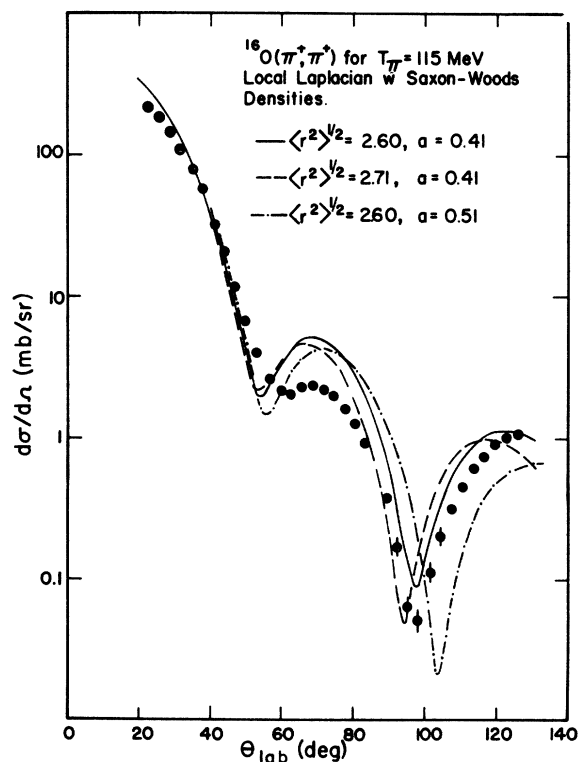


FIG. 10. Comparison of optical-model predictions of elastic scattering to recent SIN data (Ref. 20) for different density parameters. The parameters used in the calculations correspond to results between those of the dashed and dot-dashed curves.

mass region have also become available, so that several calculations have been revised to include those results.

A preliminary angular distribution for elastic scattering of positive pions on ^{16}O has recently become available from SIN²⁰ at $T_\pi = 115$ MeV. Because all of the remaining data available for ^{16}O was outside our energy range, we chose not to optimize the first-order potential strength parameters but instead adjust the nuclear density and correlation parameters. For energies above ~ 100 MeV, the first-order optical potential describes elastic-scattering data rather well using strengths determined from free πN amplitudes. Thus, after determining the nuclear density parameters at 115 MeV, we took the energy dependence determined from the free πN amplitudes.

Figure 10 shows optical-model predictions for the elastic scattering obtained with the Kisslinger and Laplacian potentials for a range of Woods-Saxon density distributions. Although it is possible to reproduce the overall shape with $\langle r^2 \rangle^{1/2} = 2.60$ fm and $a = 0.41$ fm, we have used $\langle r^2 \rangle^{1/2} = 2.72$ fm with half-value radius $R = 1.10A^{1/3}$ fm and diffuseness $a = 0.45$ fm as the best representation of the data, accepting the larger rms radius as representative, among other things, of the finite range of the pion-nucleon interaction. The complete density applicable for the DCE calcula-

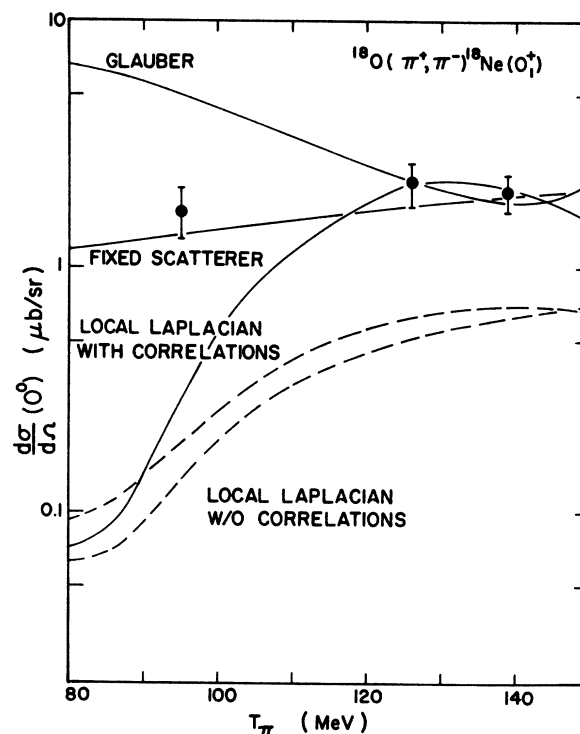


FIG. 11. Comparison of the most recent calculations with the data of this experiment.

tions for ^{18}O was then obtained by assuming the following relationships between rms radii in ^{16}O and ^{18}O :

$$r_z(^{16}\text{O}) = r_N(^{16}\text{O}) = r_z(^{18}\text{O}).$$

The neutron radius in ^{18}O was not determined but allowed to vary about a half-value radius $R_N = 1.10(1 + \delta)A^{1/3}$ for $\delta = 0$ and ± 0.05 in the calculations to show its sensitivity.

Figure 11 provides a comparison of the data of Table IV with the latest predictions. The dashed curves in this figure result from using the Saxon-Woods density with the local Laplacian potential when the half-value radius R for the neutrons was varied by 5%. The upper curve has $\delta = 0$ and gives results which are very similar to those obtained with oscillator densities. Increasing the neutron radius by 5% puts a bump in the surface region of the neutron density, which is probably a better representation since the two excess neutrons are in the s - d shell. This reduces the cross section in the region below 150 MeV as shown by the lowest dashed curve in Fig. 11. Since similar results are obtained with the Kisslinger potential, one can conclude that the first-order optical equations are not a complete representation for this nucleus, i.e., that higher-order processes¹² contribute significantly to the reaction.

These can be of various types, such as diagonal inelastic scattering, by which we mean noncharge-exchange inelastic scattering, of the π^+ , π^0 , or π^- out of and back into the channel corresponding to its appropriate member of the ground-state isospin multiplet, or possibly nondiagonal inelastic-charge exchange, i.e., all of the basic processes which are either ignored or only taken into account in an average way in the coherent scattering approximation.^{11,12} Because at least two πN encounters are involved in DCE, it is important to note that such processes include ground-state correlations of the pairing type. We do not go into detail here, but within certain approximations¹² there is basically only one free parameter to vary to fit the elastic data — the off-shell cutoff λ on the πn amplitude.^{10,21} We have varied λ about a value of 1.5 fm^{-1} as suggested by Gibbs *et al.*¹⁸ and find a best fit with $\lambda = 0.7 \text{ fm}^{-1}$; this value is used in the optical-model calculations of Fig. 11. The radius also had to be increased somewhat, consistent with the expected direction of polarization corrections, to obtain a fit comparable in quality to that obtained without correlations.

As Fig. 11 shows, inclusion of correlation effects again has the effect of increasing the DCE cross section relative to the first-order predictions and bringing them more in line with the data. The overall trend of the various optical predictions

is in the form of a broad bump in this energy region with the pion-nucleon s - p interference dip at the lower energies being too pronounced and probably the main source of the discrepancy. If one uses a more realistic first-order potential such as that of Londergan, McVoy, and Moniz,²² the effect will be to remove this dip at the lower energies with virtually no changes at the higher energies.^{12,23} Thus, a reasonably good case for sensitivity to two-nucleon correlations can be made.

The best correspondence with the data in Fig. 11 is exhibited by the fixed-scatterer approximation.¹⁰ The particular calculation we have shown is based on a Monte Carlo average of the pion amplitude over the nuclear density in which a larger radius for the neutron distribution and an improved wave function (non-Gaussian) for the unpaired neutrons was used.

V. DISCUSSION

In the foregoing sections, we have presented the experimental 0° excitation function for DCE on ^{18}O leading to the double analog and argued that this may also show the basic trend of the integrated cross section. The data show a flat distribution which is reproduced reasonably well by the latest calculations except at the lower energies where (1) the Glauber model should not be applicable, even for elastic scattering²⁴ according to most standard criteria and (2) the first-order optical equations are overly influenced by a somewhat artificial s - p pion-nucleon interference effect. Since the first-order optical equations disagree significantly with the measured cross sections, this implies sensitivity to second-order corrections such as two-nucleon correlations in the ground state.

The theoretical discussion above concentrated on the mechanism in the $^{18}\text{O}(\pi^+, \pi^-)^{18}\text{Ne}$ reaction, since that should be understood before such reactions can be used to provide a reliable spectroscopic tool. As a result, the models used to describe the nuclei were simple, i.e., two nucleons outside a closed ^{16}O core so that the usual first-order optical equations did not allow a $\Delta T = 2$, $^{16}\text{O}(\pi^+, \pi^-)^{16}\text{Ne}$ reaction. However, since the ratio of cross sections, $^{18}\text{O}/^{16}\text{O} = 2.3 \pm 0.7$, is surprisingly small, this assumption requires separate consideration.

A possible explanation of the ratio can be found in the nuclear structure of the states involved. Shell-model calculations provide reasonable wave functions and indicate the presence of substantial particle-hole admixtures in ^{16}O as well as the other nuclei being considered. An estimate²⁵ using the im-

pulse approximation, the plane-wave Born approximation, closure, and the assumption that distortion effects are comparable in both reactions resulted in the value of 3 for the $^{18}\text{O}/^{16}\text{O}$ ratio in reasonable agreement with the experiment. Within this framework, several comments regarding these reactions were made: (1) cross-shell transitions (e.g., $p^2 \rightarrow d^2$) are weaker than in-shell (e.g., $d^2 \rightarrow d^2$) transitions but are significant; (2) configuration mixing and the positive coherence of various terms as in the pairing model result in an increased cross section for ^{18}O as well as for ^{16}O DCE (a form of collectivity); and (3) the orthogonality of nuclear states results in destructive interference so that the amplitude for excited 0^+ states is greatly diminished.

In conclusion, the present work has provided the first definitive measurement of the long-discussed pion double-charge-exchange reaction, shown the existence of nonanalog transitions, determined a new nuclear mass, ^{16}Ne , and indicated the possi-

ble utility of pion DCE as a tool for study of nuclear structure. The magnitude of the ^{16}O DCE, $\Delta T = 2$ reaction indicates that (π^-, π^+) studies are also feasible. Nonanalog transitions can produce nuclei far from the line of stability, but it would appear that the present poor resolution obtained for low cross-section pion-induced reactions makes DCE a less-than-optimal tool for establishing nuclear masses if an alternative probe is available.

ACKNOWLEDGMENTS

We acknowledge the collaboration of J. Amato and J.-P. Perroud in the initial design and development of this experiment. We also thank the staff of the Clinton P. Anderson Meson Physics Facility (LAMPF) for their cooperation. This research was supported in part by the U.S. Energy Research and Development Agency and by the National Science Foundation.

-
- ¹The first discussion of pion double-charge exchange appears to have been between S. D. Drell, H. J. Lipkin, and A. de-Shalit in December 1961 (see R. G. Parsons *et al.*, Ref. 2) following the discovery of isobaric analog states. This subject was also discussed from a somewhat different perspective by T. E. O. Ericson, in Proceedings of the 1963 International Conference on High Energy Physics and Nuclear Structure [CERN Report No. 63-28, 1963 (unpublished)].
- ²A. K. Kerman and R. K. Logan, Argonne National Laboratory Report No. ANL-6848, 1964 (unpublished); R. G. Parsons, J. S. Trefil, and S. D. Drell, *Phys. Rev.* **138**, B847 (1965); S. Barshay and G. E. Brown, *Phys. Lett.* **16**, 165 (1965); T. Kohmura, *Prog. Theor. Phys.* **33**, 480 (1965); D. S. Koltun and A. Reitan, *Phys. Rev.* **139**, B1372 (1965); and F. Becker and Z. Maric, *Nuovo Cimento* **36**, 1395 (1965).
- ³J. D. Anderson and C. Wong, *Phys. Rev. Lett.* **7**, 250 (1961); see also *ibid.* **8**, 442 (1962).
- ⁴L. Gilly, M. Jean, R. Meunier, M. Spighel, J. P. Stroot, P. Duteil, and A. Rode, *Phys. Lett.* **11**, 244 (1964); P. E. Boynton, T. J. Devlin, J. Solomon, and V. Perez-Mendez, *Phys. Rev.* **174**, 1083 (1968); and C. J. Cook, M. E. Nordberg, and R. L. Burman, *ibid.* **174**, 1374 (1968).
- ⁵G. T. Garvey, J. Cerny, and R. H. Pehl, *Phys. Rev. Lett.* **12**, 726 (1964).
- ⁶Y. Shamai, J. Alster, D. Ashery, S. Cochavi, M. A. Moinester, A. I. Yavin, E. D. Arthur, and D. M. Drake, *Phys. Rev. Lett.* **36**, 82 (1976).
- ⁷T. Marks, M. P. Baker, R. L. Burman, M. D. Cooper, R. H. Heffner, R. J. Holt, D. M. Lee, D. J. Malbrough, B. M. Preedom, R. P. Redwine, J. E. Spencer, and B. Zeidman, *Phys. Rev. Lett.* **38**, 149 (1977).
- ⁸R. J. Holt, B. Zeidman, T. Marks, D. J. Malbrough, B. M. Preedom, M. P. Baker, R. L. Burman, M. D. Cooper, R. H. Heffner, D. M. Lee, R. P. Redwine, and J. E. Spencer, *Phys. Lett.* **69B**, 55 (1977).
- ⁹C. Perrin, J.-P. Albanese, R. Corfu, J.-P. Egger, P. Gretillat, C. Lunke, J. Piffaretti, E. Schwarz, J. Jansen, and B. M. Preedom, *Phys. Lett.* **69B**, 301 (1977).
- ¹⁰W. B. Kaufman, J. C. Jackson, W. R. Gibbs, *Phys. Rev. C* **9**, 1340 (1974); and W. R. Gibbs, B. F. Gibson, A. T. Hess, and G. J. Stephenson (private communication).
- ¹¹L. C. Liu and V. Franco, *Phys. Rev. C* **11**, 760 (1975).
- ¹²G. A. Miller and J. E. Spencer, *Phys. Lett.* **53B**, 329 (1974); *Ann. Phys. (N.Y.)* **100**, 562 (1976).
- ¹³R. L. Burman, R. L. Fulton, and M. Jakobson, *Nucl. Instrum. Methods* **131**, 29 (1975).
- ¹⁴B. J. Dropesky, G. W. Butler, C. J. Orth, R. A. Williams, G. Friedlander, M. A. Yates, and S. B. Kaufman, *Phys. Rev. Lett.* **34**, 821 (1975).
- ¹⁵K. L. Brown, F. Rothacker, D. C. Carey, and C. Iselin, TRANSPORT. Stanford Linear Accelerator Report No. SLAC-91, Rev. 1, 1974 (unpublished).
- ¹⁶S. Maripuu, *At. Data Nuclear Data Tables* **17**, 474 (1976); I. Kelson and G. T. Garvey, *Phys. Lett.* **23**, 689 (1966); see also E. G. Adelberger, A. V. Nero, and A. B. MacDonald, *Nucl. Phys.* **A143**, 97 (1970).
- ¹⁷G. J. KeKelis, M. S. Zisman, D. K. Scott, R. Jahn, D. J. Vieira, J. Cerny, and F. Ajzenberg-Selove, *Bull. Ann. Phys. Soc.* **22**, 552 (1977).
- ¹⁸W. R. Gibbs, B. F. Gibson, A. T. Hess, and G. J. Stephenson, Jr., *Phys. Rev. Lett.* **36**, 85 (1976); and private communication.
- ¹⁹M. K. Gupta and G. E. Walker, *Nucl. Phys.* **A256**, 444 (1976).
- ²⁰E. Boschitz, J. Arvieux, J.-P. Albanese, Q. Ingram, L. Pflug, and J. Zichy (private communication).
- ²¹B. Goplen, W. R. Gibbs, and E. Lomon, *Phys. Rev.*

Lett. 32, 1012 (1974).

²²J. T. Londergan, K. W. McVoy, and E. J. Moniz, Ann. Phys. (N.Y.) 86, 147 (1974).

²³G. A. Miller (private communication).

²⁴C. Schmit, Nuovo Cimento Lett. 4, 454 (1970);

C. Wilkin, *ibid.* 4, 490 (1970); and J. P. Maillet, C. Schmit, and J. P. Dedonder, *ibid.* 5, 191 (1971).

²⁵T. S. H. Lee, D. Kurath, and B. Zeidman, Phys. Rev. Lett. 39, 1307 (1977).